

Carrier-induced ferromagnetism in a diluted Hubbard model

Sudhakar Pandey and Avinash Singh*

Department of Physics, Indian Institute of Technology Kanpur - 208016

Carrier-induced ferromagnetism is investigated in a diluted Hubbard model for ordered impurity arrangements. The delicate competition between particle-hole processes contributing to the spin couplings results in a rich variety of behaviour. The ferromagnetic transition temperature obtained within the spin-fluctuation theory is in good agreement with reported values for $\text{Ga}_{1-x}\text{Mn}_x\text{N}$.

I. INTRODUCTION

The recent discovery of ferromagnetism in diluted magnetic semiconductors (DMS) such as $\text{Ga}_{1-x}\text{Mn}_x\text{As}$ ^{1,2} and $\text{Ga}_{1-x}\text{Mn}_x\text{N}$,³ and the intensive efforts to increase the ferromagnetic transition temperature in view of potential technological applications, has generated tremendous interest in the novel ferromagnetism exhibited by these systems in which magnetic interaction between localized spins is mediated by doped carriers.^{4,5,6,7,8,9,10,11,12,13,14,15,16,17,18,19} The nature of the ferromagnetic state has also attracted much attention, particularly in the context of competing antiferromagnetic (AF) interaction which result in noncollinear ordering, spin-glass behaviour, and significant sensitivity of spin stiffness and transition temperature T_c on carrier concentration, spin clustering etc.

DMS are mixed spin-fermion systems, involving randomly distributed localized magnetic impurities (e.g., Mn^{++} , having $S = 5/2$) and mobile carriers (e.g., holes) in the semiconductor band. With carrier concentration p much smaller than the magnetic impurity concentration x , the DMS systems provide a complimentary limit to Kondo systems. Conventionally, the coupling between localized impurity spin \mathbf{S} and mobile valence band holes is represented by the exchange interaction $-J\mathbf{S}\cdot\boldsymbol{\sigma}$, where $\boldsymbol{\sigma} = \Psi^\dagger[\boldsymbol{\sigma}]\Psi$ is the fermion spin operator.

Cuprates form another class of strongly correlated systems in which the concentration of doped carriers is small in comparison to that of (Cu) spins. Extensively studied within the Hubbard model, the dominant interaction in cuprates is the AF exchange interaction between neighbouring Cu spins, and AF spin correlations persist even for small hole doping. Against this strong tendency for AF ordering, the delocalization energy gain of doped carriers, which favours parallel spin alignment, results in only a marginal twisting of spins, as in the proposed spiral phases.^{20,21} It is therefore interesting that elimination of the strong AF spin interaction in a *diluted* Hubbard model,¹⁷ with no direct hopping between relatively distant impurity spins, does indeed lead to a ferromagnetic state stabilized by carrier-induced spin couplings.

The spin stiffness in the ferromagnetic state of the diluted Hubbard model goes through a maximum with respect to both doping concentration p and the interaction strength U . This optimization behaviour can be qualitatively understood in terms of a competition between the increasing magnitude of carrier spin polarization $\chi(U)$

and the increasing rapidity of its oscillation, which limits the growth of the spin coupling $U^2\chi_{ij}(U)$ between two magnetic impurities at a fixed separation. Similar behaviour was observed in the spin-fermion model for the effective ferromagnetic coupling $J_{ij} = J^2\chi_{ij}(J)$ in terms of the generalized spin response $\chi(J)$ for finite J .¹⁷ As $\chi(J)$ involves particle-hole processes, the spin couplings identically vanish in the absence of doping. However, in the diluted Hubbard model, even with no carrier doping ($p = 0$) in the majority-spin band, particle-hole processes involving the empty minority-spin impurity band result in antiferromagnetic spin couplings, which destabilize the ferromagnetic state below a critical doping concentration.

In this paper, we study the novel ferromagnetic state of the diluted Hubbard model for *ordered* impurity arrangements. We focus on magnon excitations and the spin stiffness, which provide quantitative measures of the stability and spin couplings in the ferromagnetic state, as well as the transition temperature in three dimensions. While preliminary real-space studies for both ordered and disordered impurity arrangements were carried out earlier on three-dimensional finite-size lattices,¹⁷ use of \mathbf{k} -space representation in this paper allows for much larger lattices, thus permitting a more refined study of the competing spin interactions with respect to carrier concentration, impurity separation, interaction strength, and wave vector. Indeed, the antiferromagnetic - ferromagnetic quantum phase transition stands out as a significantly prominent feature in the low doping regime. AF-F and spin-glass transitions at low doping have actually been observed in Mn-doped II-VI semiconductors.^{22,23,24} With increasing doping concentration, an anomalous increase in the spin stiffness is observed which involves, as explained in section III B, a subtle interplay of impurity moment reduction, impurity character of doped states, and competing particle-hole processes, all characteristics of the itinerant ferromagnetic state.

Within the relatively simpler ferromagnetic Kondo lattice model (FKLM), in which a localized spin is present at every lattice site, magnon excitations have been studied recently, as a function of electron density n in the conduction band and the spin-fermion coupling J , in the context of heavy fermion materials,²⁵ ferromagnetic metals Gd, Tb, Dy, doped EuX,²⁶ and manganites.^{27,28,29} Magnon dispersion has also been obtained in the context of DMS.^{30,31,32,33} However, a uniform impurity-induced Zeeman splitting of the carrier spin bands is assumed.^{30,31,33}

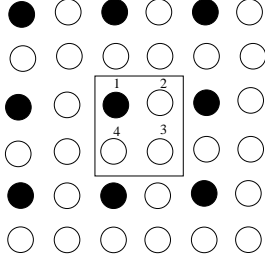


FIG. 1: An ordered arrangement of impurity atoms (●) on a square host lattice (○). Also shown are the sublattice labels corresponding to the four distinct sites within the unit cell.

II. DILUTED HUBBARD MODEL

We consider a diluted Hubbard model

$$H = t \sum_{i,\delta,\sigma} a_{i,\sigma}^\dagger a_{i+\delta,\sigma} + t' \sum_{I,\delta,\sigma} a_{I,\sigma}^\dagger a_{I+\delta,\sigma} + \epsilon_d \sum_{I,\sigma} a_{I\sigma}^\dagger a_{I\sigma} + U \sum_I (n_{I\uparrow} - \langle n_I \rangle)(n_{I\downarrow} - \langle n_I \rangle) \quad (1)$$

on square and cubic lattices with nearest-neighbour (NN) hopping between sites i and $i + \delta$. Here I refers to the impurity sites, ϵ_d is the impurity on-site energy, and $\langle n_I \rangle = \langle n_{I\uparrow} + n_{I\downarrow} \rangle / 2$ is the spin-averaged impurity density. The energy-scale origin is set so that the host on-site energy is zero, and we take the impurity level to lie at the top of the host band ($\epsilon_d = 2dt = W/2$ in d dimensions) to optimize local-moment formation. For a positive sign of the hopping term, the top of the host band lies at $\mathbf{k} = 0$, as in the valence band of DMS. For simplicity, we take the same hopping ($t' = t$) between the host-host and host-impurity pairs of sites. Higher spin magnetic impurities, such as the $S = 5/2$ Mn impurities in $\text{Ga}_{1-x}\text{Mn}_x\text{As}$, can be realistically represented within a generalized Hubbard model involving multiple orbitals per site.³⁴

A. Hartree-Fock ferromagnetic state

In the Hartree-Fock (HF) approximation, the interaction term reduces to a magnetic coupling

$$H_{\text{int}}^{\text{HF}} = - \sum_I \boldsymbol{\sigma}_I \cdot \boldsymbol{\Delta}_I \quad (2)$$

with the local mean field $\boldsymbol{\Delta}_I$, resembling the semi-classical limit of the exchange interaction $-\sum_I J \boldsymbol{\sigma}_I \cdot \mathbf{S}_I$ in the spin-fermion model. Here the impurity spin operator $\boldsymbol{\sigma}_I = \Psi_I^\dagger [\boldsymbol{\sigma}] \Psi_I$ in terms of the fermionic field operator $\Psi_I = \begin{pmatrix} a_{I\uparrow} \\ a_{I\downarrow} \end{pmatrix}$. The mean field $\boldsymbol{\Delta}_I$ is self-consistently determined from the ground-state expectation value:

$$2\boldsymbol{\Delta}_I = \langle \boldsymbol{\sigma}_I \rangle U. \quad (3)$$

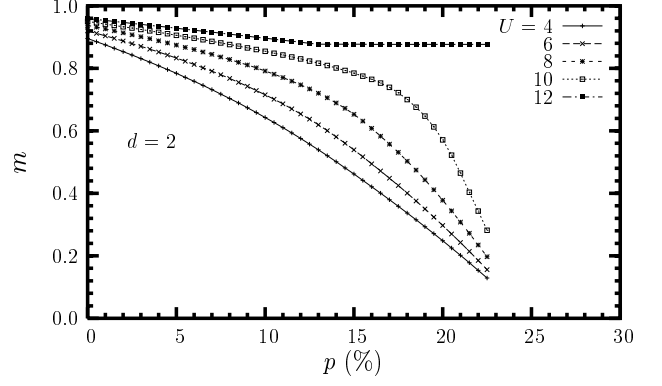


FIG. 2: Variation of impurity magnetization with hole concentration for the two-dimensional case ($x = 25\%$). With increasing U , the impurity character of majority-spin states at the top of the band diminishes, and the impurity moment is therefore less susceptible to hole doping.

B. Sublattice-basis representation

We consider ordered (superlattice) arrangements of magnetic impurities on square and cubic host lattices, with impurity separations of $2a$ and $3a$. Translational symmetry within the sublattice basis conveniently allows Fourier transformation to momentum space. For concreteness, we consider a square host lattice in the following, with magnetic impurities placed at every other host site, corresponding to superlattice spacing $2a$ and impurity concentration $x = 25\%$. There are four sublattices, numbered $\alpha = 1, 2, 3, 4$, corresponding to the four sites in the unit cell, as shown in Fig. 1. We choose length and energy units such that the lattice spacing $a = 1$ and the hopping term $t = 1$.

Without loss of generality, we assume a mean field $\boldsymbol{\Delta}_I = \Delta \hat{z}$ in the z direction. Fourier transformation within the four-sublattice basis yields the HF Hamiltonian

$$H_{\text{HF}}^\sigma = \sum_{\mathbf{k}} \Psi_{\mathbf{k}\sigma}^\dagger \begin{bmatrix} \epsilon_d - \sigma \Delta & \epsilon_{\mathbf{k}}^x & 0 & \epsilon_{\mathbf{k}}^y \\ \epsilon_{\mathbf{k}}^x & 0 & \epsilon_{\mathbf{k}}^y & 0 \\ 0 & \epsilon_{\mathbf{k}}^y & 0 & \epsilon_{\mathbf{k}}^x \\ \epsilon_{\mathbf{k}}^y & 0 & \epsilon_{\mathbf{k}}^x & 0 \end{bmatrix} \Psi_{\mathbf{k}\sigma} \quad (4)$$

for spin σ , where $\epsilon_{\mathbf{k}}^x = 2t \cos k_x$ and $\epsilon_{\mathbf{k}}^y = 2t \cos k_y$ correspond to hopping terms in the x and y directions, respectively. Here the field operator $\Psi_{\mathbf{k}\sigma} = (a_{\mathbf{k}\sigma}^1, a_{\mathbf{k}\sigma}^2, a_{\mathbf{k}\sigma}^3, a_{\mathbf{k}\sigma}^4)$ defines the sublattice basis, where $a_{\mathbf{k}\sigma}^\alpha$ refers to the fermion operator for sublattice index α . Generalization to other impurity concentrations and dimensions is straightforward. Hopping terms to the right (up) and left (down) do not connect the same sublattice in general, yielding a Hermitian Hamiltonian matrix with hopping terms $te^{\pm i k_x}$ etc. The case of impurity spacing 2 is, however, special as hopping terms in opposite directions do connect the same sublattice, yielding a real symmetric Hamiltonian matrix.

The HF Hamiltonian matrix is numerically diagonal-

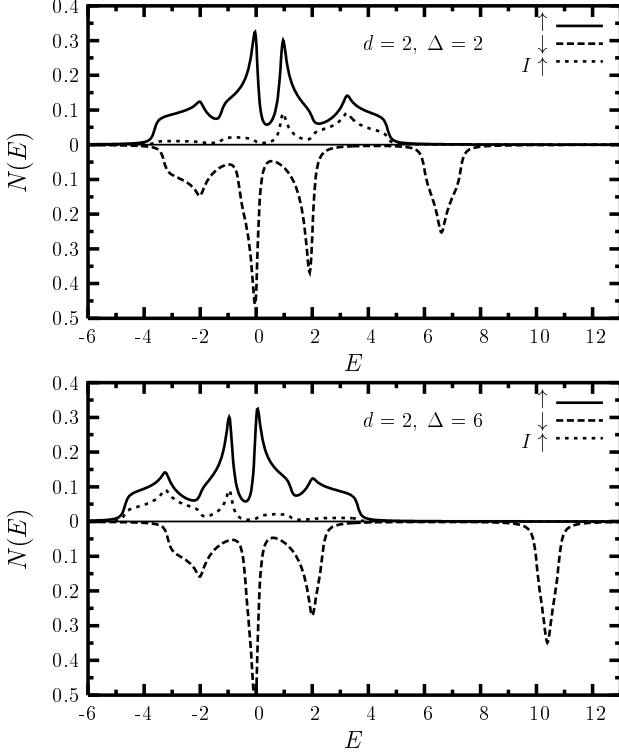


FIG. 3: Total and impurity (I) density of states for the 2-d case ($x = 25\%$) for two values of the mean field Δ , showing the split-off impurity band and the impurity-induced sub-bands.

ized to obtain the four eigenvalues $E_{\mathbf{k}\sigma}^\mu$, corresponding to the four sub-bands $\mu = 1, 2, 3, 4$ in increasing order of energy. The four-component eigenvectors $\phi_{\mathbf{k}\sigma}^{\mu\alpha}$ yield the amplitude on sublattice α . Summing over occupied states yields the impurity magnetization and the self-consistency condition

$$\frac{2\Delta}{U} = m(\Delta) = \langle \sigma_I^z \rangle = \sum_{\mathbf{k}, \mu}^{E_{\mathbf{k}\sigma}^\mu < E_F} (\phi_{\mathbf{k}\uparrow}^{\mu\alpha=1})^2 - (\phi_{\mathbf{k}\downarrow}^{\mu\alpha=1})^2. \quad (5)$$

Variation of the impurity magnetization m with doping concentration p is shown in Fig. 2.

C. Quasiparticle spectrum

Each magnetic impurity contributes two spin states. The minority-spin impurity state (energy $\epsilon_d + \Delta$) is pushed up by the local Coulomb repulsion, and forms a split-off narrow impurity band due to the small overlap with neighbouring impurity states. The majority-spin impurity state (energy $\epsilon_d - \Delta$) mixes with the host band states for $\epsilon_d - \Delta \ll W$, and splits off on the low-energy side for large Δ . Figures 3 and 4 show a comparison of the quasiparticle density of states $N(E)$ for two Δ values for the 2-d and 3-d cases, showing the four and eight sub-bands corresponding to the sublattices, respectively.

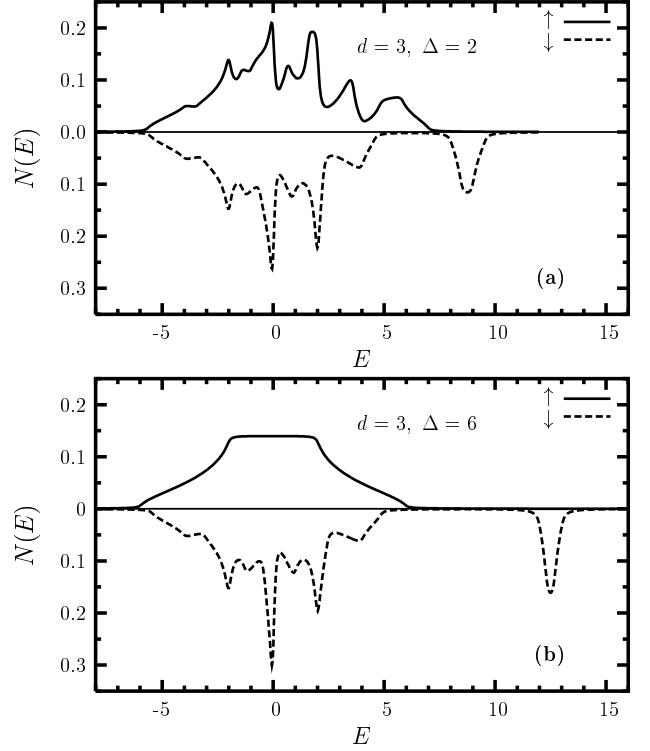


FIG. 4: Density of states for the 3-d case ($x = 12.5\%$) for two values of the mean field Δ .

For minority spin, while the impurity band shifts up with increasing Δ and narrows due to decreasing effective impurity hopping $t_{\text{eff}} \sim t^2/(\epsilon_d + \Delta)$, the host sub-bands remain unaffected reflecting strong host-impurity decoupling. The majority-spin sub-bands, however, are pulled down in energy by the exchange interaction, decreasing the energy separation between the two bands. With increasing Δ , the impurity character of majority-spin states at the top of the band diminishes, as seen in Fig. 3.

In the undoped insulating state, the Fermi energy lies in the gap between the top of the majority-spin valence band and the minority-spin impurity band. The empty impurity band ensures local-moment formation on each impurity site. Carrier doping is introduced by adding holes to the top of the majority-spin band. The mean field Δ decreases with doping concentration p , which shifts the majority-spin band to the right. The Fermi energy therefore remains above the minority-spin valence sub-band ($\mu = 3$ or 7), yielding a finite Stoner gap for low doping.

III. TRANSVERSE SPIN FLUCTUATIONS

Transverse spin fluctuations are gapless, low-energy excitations in the broken-symmetry state of magnetic systems possessing continuous spin-rotation symmetry. Therefore, at low temperatures they play an important role in diverse macroscopic properties such as existence

of long-range order, spin stiffness magnitude and temperature dependence of magnetization, transition temperature, spin correlation etc.

We study the time-ordered, transverse spin propagator

$$\chi_{ij}^{+-}(t-t') = i\langle\Psi_G|T[S_i^+(t)S_j^-(t')]\Psi_G\rangle \quad (6)$$

in the the ferromagnetic ground state $|\Psi_G\rangle$, involving the spin-raising (S_i^+) and spin-lowering (S_j^-) operators at sites i and j . In the random phase approximation (RPA), the magnon propagator

$$[\chi^{+-}(\mathbf{q}, \omega)] = [\chi^{-+}(-\mathbf{q}, -\omega)] = \frac{[\chi^0(\mathbf{q}, \omega)]}{1 - [U][\chi^0(\mathbf{q}, \omega)]} \quad (7)$$

in \mathbf{q}, ω space, where the zeroth-order, particle-hole propagator $[\chi^0(\mathbf{q}, \omega)]$ is obtained by integrating out the fermions in the self-consistent broken-symmetry state. In the sublattice basis we have

$$\begin{aligned} [\chi^0(\mathbf{q}, \omega)]_{\alpha\beta} &= i \int \frac{d\omega'}{2\pi} \sum_{\mathbf{k}} [G^\uparrow(\mathbf{k}, \omega')]_{\alpha\beta} [G^\downarrow(\mathbf{k}', \omega' + \omega)]_{\beta\alpha} \\ &= \sum_{\substack{E_{\mathbf{k}'\downarrow}^\nu > E_F \\ E_{\mathbf{k}\uparrow}^\mu < E_F}} \frac{\phi_{\mathbf{k}\uparrow}^{\mu\alpha} \phi_{\mathbf{k}\uparrow}^{\mu\beta*} \phi_{\mathbf{k}'\downarrow}^{\nu\beta} \phi_{\mathbf{k}'\downarrow}^{\nu\alpha*}}{E_{\mathbf{k}'\downarrow}^\nu - E_{\mathbf{k}\uparrow}^\mu - \omega} \\ &+ \sum_{\substack{E_{\mathbf{k}\uparrow}^\mu > E_F \\ E_{\mathbf{k}'\downarrow}^\nu < E_F}} \frac{\phi_{\mathbf{k}\uparrow}^{\mu\alpha} \phi_{\mathbf{k}\uparrow}^{\mu\beta*} \phi_{\mathbf{k}'\downarrow}^{\nu\beta} \phi_{\mathbf{k}'\downarrow}^{\nu\alpha*}}{E_{\mathbf{k}\uparrow}^\mu - E_{\mathbf{k}'\downarrow}^\nu + \omega}, \end{aligned} \quad (8)$$

where $\mathbf{k}' \equiv \mathbf{k} + \mathbf{q}$. In Eq. (7), the diagonal interaction matrix $[U]_{\alpha\alpha} = U\delta_{\alpha 1}$ has non-zero element only on the impurity sublattice $\alpha = 1$. It is therefore convenient to write

$$[\chi^{+-}(\mathbf{q}, \omega)] = \frac{1}{[A(\mathbf{q}, \omega)]} - \frac{1}{[U]} \quad (9)$$

in terms of a matrix $[A(\mathbf{q}, \omega)] = [U] - [U][\chi^0(\mathbf{q}, \omega)][U]$, which has non-vanishing matrix elements only on the impurity sublattice. Magnon-mode energies $\omega_{\mathbf{q}}$ are therefore obtained from the magnon pole condition

$$1 - U\chi^0(\mathbf{q}, \omega_{\mathbf{q}}) = 0, \quad (10)$$

where $\chi^0(\mathbf{q}, \omega)$ represents the impurity-sublattice matrix element of $[\chi^0(\mathbf{q}, \omega)]_{\alpha\beta}$. In the ferromagnetic state, typically $\chi^0(\mathbf{q}, \omega) = \frac{1}{\mathcal{B}} - \mathcal{A}q^2 + \mathcal{B}\omega$ for small q, ω , so that the magnon energy $\omega_{\mathbf{q}} = (\mathcal{A}/\mathcal{B})q^2$. The coefficient \mathcal{A} is a measure of the spin stiffness, whose sign determines the stability of the HF ferromagnetic state with respect to transverse fluctuations, as discussed below.

A. Stability of the ferromagnetic state

The undoped state, with filled majority-spin states and an empty minority-spin impurity band, amounts to a half-filled case with respect to magnetic impurities. Virtual hopping between impurity sites therefore generates

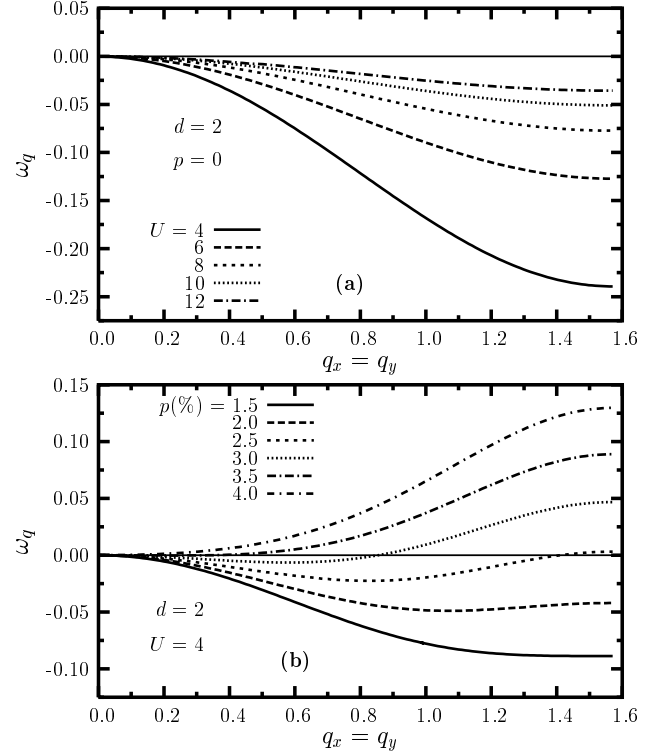


FIG. 5: (a) Negative magnon energy in the absence of hole doping indicates instability of the ferromagnetic state due to antiferromagnetic spin couplings, which weakened with increasing U . (b) Stabilization of the ferromagnetic state with increasing hole concentration.

antiferromagnetic exchange interaction t_{eff}^2/U between neighbouring magnetic impurities, resulting in antiferromagnetic ordering. The carrier-mediated ferromagnetic couplings are absent, and the self-consistent ferromagnetic state is therefore unstable and actually represents a saddle point. The instability is reflected in a negative sign of the coefficient \mathcal{A} (spin stiffness), which makes the transverse response eigenvalue $U\chi^0(\mathbf{q}) > 1$ and yields negative magnon energies [Fig. 5(a)]. With hole doping, ferromagnetic coupling strengthens, long-wavelength magnon-mode energy changes sign, and ferromagnetic ordering is stabilized at some critical hole concentration [Fig. 5(b)]. Thus the diluted Hubbard model is characterized by an AF - F transition at a finite doping concentration, which is more prominent for small U .

A significant feature of Fig. 5(b) is the distinct behaviour of long- and short-wavelength magnon modes. Even in the unstable regime, with negative-energy long-wavelength modes, the zone-edge modes ($q_x, q_y \sim \pi/2$) may have positive energy, thereby giving a spurious indication of stability. Incorporating only the zone-edge (Ising) excitations, the dynamical mean-field theory is therefore insensitive to the non-trivial long-wavelength behaviour arising from competing spin couplings.

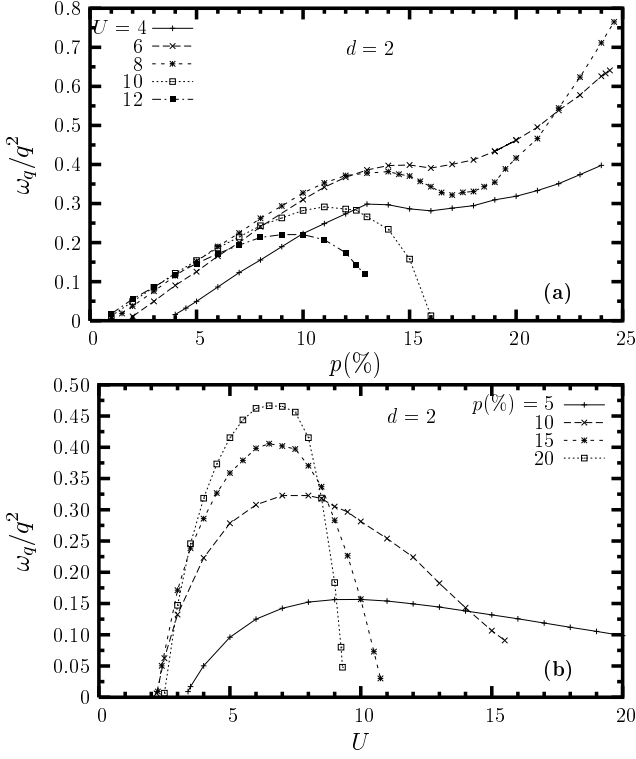


FIG. 6: Variation of spin stiffness with (a) hole concentration and (b) interaction strength U , for the 2-d case ($x = 25\%$).

B. Spin stiffness

The long-wavelength magnon-mode energy $\omega_{\mathbf{q}}$ and spin stiffness $\omega_{\mathbf{q}}/q^2$ provide a composite measure of impurity spin couplings in the carrier-mediated ferromagnetic state. Figures 6 and 7 show the behaviour of spin stiffness with doping concentration p and interaction strength U for the 2-d and 3-d cases with impurity spacing 2. A minimum hole concentration to stabilize the ferromagnetic state is clearly seen, especially for low U , when the competing antiferromagnetic spin couplings are relatively stronger. The increase in spin stiffness with hole concentration exhibits the essence of carrier-mediated ferromagnetism. The initial increase is nearly linear in two dimensions and distinctly sublinear in three dimensions. The spin stiffness exhibits an optimization with respect to both p and U , which can be understood qualitatively within the generalized RKKY theory in terms of a competition between increasing magnitude of carrier-spin polarization and increasing rapidity of its oscillation.

Similar behaviour of spin stiffness is seen (Fig. 8) when impurity spacing is increased to 3 in the 2-d case. The peak spin stiffness is clearly reduced, reflecting the weakening of spin couplings with increased impurity separation. However, in the low doping regime, the spin stiffness for $x = 1/9$ is actually greater than that for $x = 1/4$ (see inset). As the stiffness must eventually decrease with increasing impurity separation, this interestingly shows an optimization behaviour with respect to impurity con-

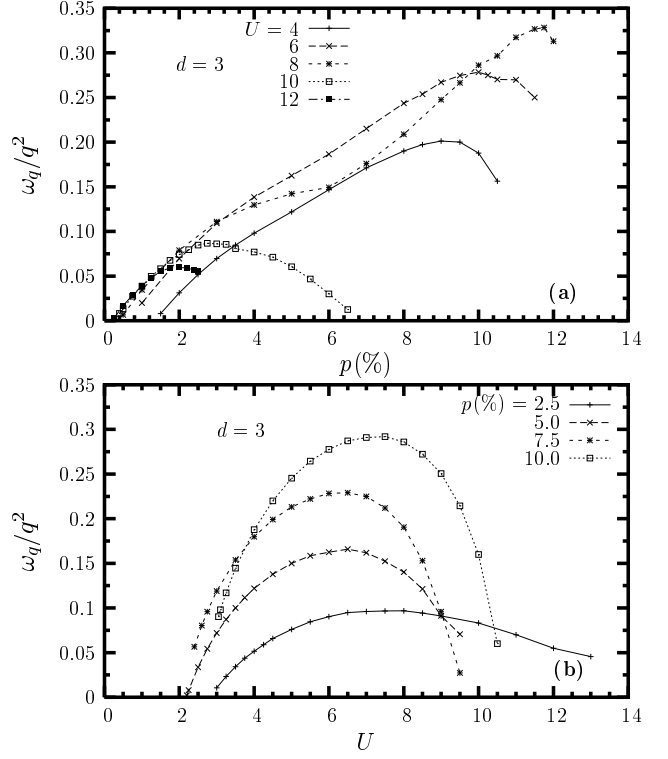


FIG. 7: Variation of spin stiffness with (a) hole concentration and (b) interaction strength U , for the 3-d case ($x = 12.5\%$).

centration x as well.

The anomalous increase at higher p , seen in Figs. 6-8 for lower U values, is due to a competition between two particle-hole processes, as discussed below. Figure 9 shows the doping dependence of $U^2[\chi^0(0) - \chi^0(\mathbf{q})]/q^2$ for the two particle-hole processes in Eq. (8), labeled as 1 and 2, which provide measures of the corresponding spin-stiffness contributions. Positive (negative) value indicates dominant ferromagnetic (antiferromagnetic) spin coupling. Process 2, which is activated only upon doping in the majority-spin band, is seen to be dominantly ferromagnetic in the low-doping regime and exhibits the typical RKKY peak behaviour before turning negative due to the oscillating carrier-spin polarization. However, process 1, which is weakly antiferromagnetic for $p \approx 0$, changes sign with doping, and becomes increasingly ferromagnetic; it is the sharp increase seen at higher doping which causes the distinct minimum feature in the total spin stiffness. This feature is more pronounced at lower U because the sharply reduced impurity moment and Δ at higher doping (see Fig. 2), cause the impurity states to be more extended, thus enhancing the process 1 stiffness.

C. Transition temperature

Determination of the magnon spectrum in the carrier-mediated ferromagnetic state allows an estimation of the transition temperature T_c for the diluted Hubbard model

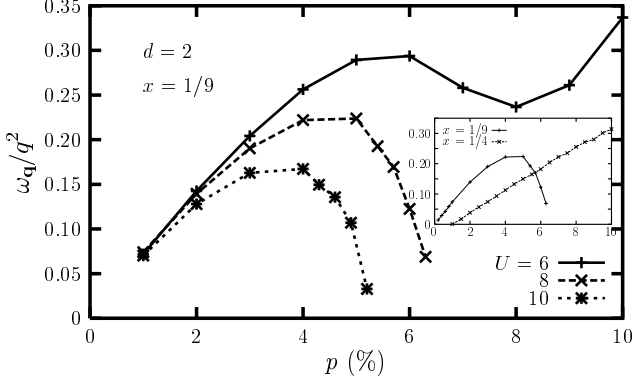


FIG. 8: Increasing the impurity spacing to 3 results in qualitatively similar but reduced peak spin stiffness. Inset shows comparison of the $x = 1/4$ and $x = 1/9$ cases for $U = 8$.

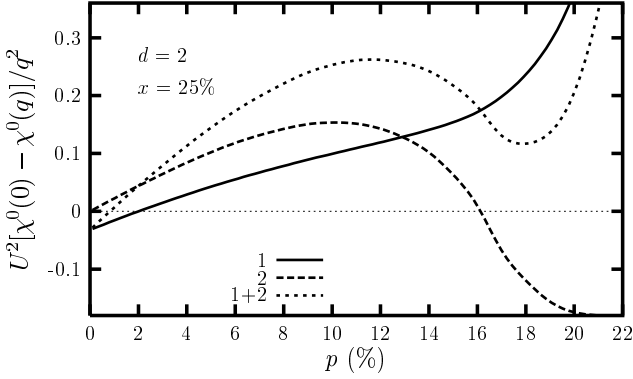


FIG. 9: Spin-stiffness contributions corresponding to the two particle-hole processes in Eq. (8), showing the distinct minimum feature and the anomalous increase arising from their competition. Here $U = 9$.

in three dimensions. As the ferromagnetic state is characterized by small spin stiffness due to strong competition between ferromagnetic and antiferromagnetic spin couplings, the dominant contribution to reduction in magnetization is from the thermal excitation of long-wavelength magnon modes. Therefore, the transition temperature T_c can be estimated in terms of an equivalent Heisenberg model with matching spin stiffness.

For a nearest-neighbour, spin- S quantum Heisenberg model with interaction energy J on a cubic lattice (coordination number $z = 6$), the magnon energy

$$\omega_{\mathbf{q}} = zJS(1 - \gamma_{\mathbf{q}}), \quad (11)$$

where $\gamma_{\mathbf{q}} = (\cos 2q_x + \cos 2q_y + \cos 2q_z)/3$, corresponding to the magnetic lattice spacing 2. Indeed, the magnon energy is maximum for $q_x = q_y = q_z = \pi/2$, as also seen in Fig. 5 for the 2-d case. Considering the small q limit of Eq. (11), and matching the spin stiffness, we obtain $D = \omega_{\mathbf{q}}/q^2 = 4JS = 2J$, where we have set $S = 1/2$

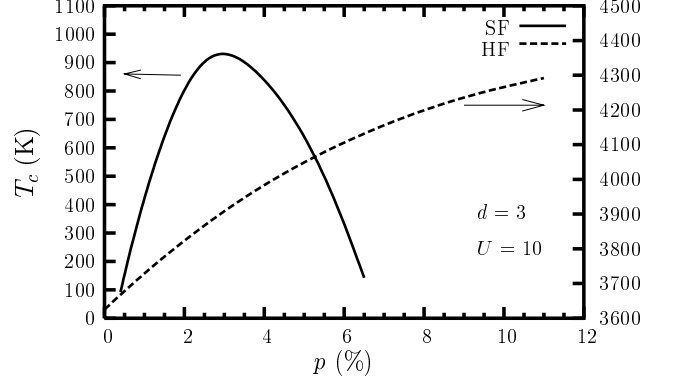


FIG. 10: Comparison of the transition temperature T_c obtained from the renormalized spin-fluctuation theory (SF) with the HF result (temperature scale on the right), highlighting the order-of-magnitude difference between the spin-ordering and moment-melting temperatures. Here $x = 12.5\%$.

for the diluted Hubbard model having a single magnetic orbital per site.

For the spin- S Heisenberg model, the transition temperature

$$T_c^{\text{SF}} = \frac{zJS(S+1)}{3} f_{\text{SF}}^{-1} = DS(S+1) f_{\text{SF}}^{-1} \quad (12)$$

within the renormalized spin-fluctuation theory is somewhat lower than the mean-field value $T_c^{\text{MF}} = zJS(S+1)/3$ due to the spin-fluctuation factor $f_{\text{SF}} = \sum_{\mathbf{q}} (1 - \gamma_{\mathbf{q}})^{-1}$, which is approximately 1.5 for the cubic lattice. Extrapolating to spin- S magnetic impurities in the diluted Hubbard model, represented by multiple magnetic orbitals per site,³⁴ with the same equivalent interaction energy $J = D/2$ as obtained above, the transition temperature reduces to the expression in Eq. (12). Taking $S = 5/2$ for Mn impurities, and a realistic heavy-hole bandwidth $W = 12t = 2$ eV, the transition temperature evaluated from Eq. (12) is shown in Fig. 8. Also shown for comparison is the HF result obtained from a finite-temperature analysis of the self-consistency condition. The HF T_c is naturally an order of magnitude higher as it really corresponds to a moment-melting temperature.

At the HF level, the impurity moment vanishes at a temperature $T \sim \Delta$, the minority-spin impurity-band energy relative to the Fermi energy. The marginal increase seen in T_c^{HF} with doping is simply due to the decreasing Fermi energy, whereas the impurity-band energy remains essentially unchanged.

Similar estimations of T_c from magnon energy were recently carried out for the ferromagnetic Kondo lattice model²⁹ and in the context of DMS,^{17,30,31,33} as a function of carrier concentration p . Optimization behaviour was found in these cases as well, with T_c increasing with p upto a maximum, followed by a monotonic decrease.

IV. CONCLUSIONS

Carrier-induced ferromagnetism was investigated in the diluted Hubbard model for ordered impurity arrangements. Momentum-space representation within the sublattice basis permitted a detailed study with respect to carrier doping, impurity spacing, electron correlation, and wave vector. The delicate competition between spin couplings results in an AF-F quantum phase transition in the low-doping regime. Competition between the increasing magnitude and increasing rapidity of oscillation of the carrier-spin polarization was observed, yielding a characteristic optimization of the spin stiffness with doping concentration p and interaction strength U . Surprisingly, in the low doping regime, the spin stiffness was found to actually increase when the impurity separation increased from 2 to 3 in the 2-d case, indicating an interesting optimization with respect to impurity concentration as well. In addition, the itinerant ferromagnetic state exhibits a subtle interplay of impurity moment reduction, impurity character of doped states, and competing particle-hole processes in the carrier-spin polarization, resulting in a distinct minimum and an anomalous increase in the spin stiffness at higher doping concentration.

For the cubic impurity arrangement, doping dependence of the ferromagnetic transition temperature T_c was calculated within the renormalized spin-fluctuation

theory from the magnon spectrum, and compared with the HF result so as to highlight the difference between spin-ordering and moment-melting temperatures. For $S = 5/2$ and a realistic heavy-hole bandwidth of 2 eV, the peak calculated T_c of 960 K at $p \approx 3\%$ is in good agreement with the highest reported T_c value of 940 K observed in $\text{Ga}_{1-x}\text{Mn}_x\text{N}$.³

While our main objective was to examine the novel ferromagnetism in the diluted Hubbard model, several features of this itinerant ferromagnetic state are of relevance to DMS systems as well. For example, impurity bands formed by overlap of Mn d orbitals are prominent features in density functional calculations within the local spin density approximation (LSDA), and a characteristic dependence of T_c on Mn concentration is obtained for impurity bands formed within the gap, as is the case for $\text{Ga}_{1-x}\text{Mn}_x\text{N}$.³⁵ Furthermore, correlation effects have also been examined recently within the LSDA+U approach³⁶ to obtain better agreement of the Mn d-DOS peak position with recent photoemission experiments.

V. ACKNOWLEDGEMENT

Helpful discussions with Indra Dasgupta are gratefully acknowledged.

* Electronic address: avinas@iitk.ac.in

- ¹ H. Ohno, A. Shen, F. Matsukara, A. Oiwa, A. Endo, S. Katsumoto, and Y. Iye, Appl. Phys. Lett. **69**, 363 (1996).
- ² F. Matsukara, H. Ohno, A. Shen, and Y. Sugawara, Phys. Rev. B **57**, R2037 (1998).
- ³ S. Sonoda *et al.*, J. Cryst. Growth **237-239**, 1358 (2002).
- ⁴ T. Dietl, A. Haury, and Y. M. d'Aubigne, Phys. Rev. B **55**, R3347 (1997).
- ⁵ M. Takahashi, Phys. Rev. B **56**, 7389 (1997).
- ⁶ H. Akai, Phys. Rev. Lett. **81**, 3002 (1998).
- ⁷ T. Jungworth, W. A. Atkinson, B. H. Lee, and A. H. MacDonald, Phys. Rev. B **59**, 9818 (1999); B. H. Lee, T. Jungworth, and A. H. MacDonald, *ibid* **61**, 15606 (2000).
- ⁸ T. Dietl, H. Ohno, F. Matsukara, J. Cibert, and D. Ferrand, Science, **287**, 1019 (2000).
- ⁹ T. Dietl, F. Matsukara, and H. Ohno, Phys. Rev. B **66**, 033203 (2002).
- ¹⁰ T. Jungworth, J. König, J. Sinova, K. Kučera, and A. H. MacDonald, Phys. Rev. B **66**, 012402 (2002).
- ¹¹ A. Chattopadhyay, S. Das Sarma, and A. J. Millis, Phys. Rev. Lett. **87**, 227202 (2001).
- ¹² S. Das Sarma, E. H. Hwang, and A. Kaminski, Phys. Rev. B **67**, 155201 (2003).
- ¹³ J. Schliemann and A. H. MacDonald, Phys. Rev. Lett. **88**, 137201 (2002).
- ¹⁴ J. Schliemann, J. König, and A. H. MacDonald, Phys. Rev. B **64**, 165201 (2001).
- ¹⁵ M. P. Kennett, M. Berciu and R. N. Bhatt, Phys. Rev. B **66**, 045207 (2002).
- ¹⁶ G. Alvarez, M. Mayr, and E. Dagotto, Phys. Rev. Lett. **89**, 277202 (2002).
- ¹⁷ A. Singh, A. Dutta, S. K. Das, and V. A. Singh, Phys. Rev. B **68**, 235208 (2003).
- ¹⁸ A. Singh, cond-mat/0307009 (2003).
- ¹⁹ C. Timm, J. Phys.: Condens. Matter **15**, R1865 (2003).
- ²⁰ H. R. Krishnamurthy, C. Jayaprakash, S. Sarker, and W. Wenzel, Phys. Rev. Lett. **64**, 950 (1990).
- ²¹ Z. Y. Weng and C. S. Ting, Phys. Rev. B **42**, 803 (1990).
- ²² A. Haury, A. Wasiela, A. Arnoult, J. Cibert, S. Tatarenko, T. Dietl, and Y. M. d'Aubigne, Phys. Rev. Lett. **79**, 511 (1997).
- ²³ D. Ferrand *et al.*, Phys. Rev. B **63**, 085201 (2001).
- ²⁴ J. K. Furdyna and J. Kossut, *Semiconductors and Semimetals*, Vol. 25 (Academic Press, New York, 1988).
- ²⁵ M. Sigrist and K. Ueda, Phys. Rev. B **46**, 175 (1992).
- ²⁶ M. Donath, P. A. Dowben, and W. Nolting (Eds.), *Correlations in Local-Moment Systems: Rare-Earth Elements and Compounds*, World Scientific, Singapore, 1998.
- ²⁷ N. Furukawa, J. Phys. Soc. Jpn. **65**, 1174 (1996).
- ²⁸ X. Wang, Phys. Rev. B **57**, 7427 (1998).
- ²⁹ M. Vogt, C. Santos, and W. Nolting, Phys. Stat. Sol. (b) **233**, 679 (2001).
- ³⁰ J. König, H. H. Lin, and A. H. MacDonald, Phys. Rev. Lett. **84**, 5628 (2000); J. König, T. Jungworth, and A. H. MacDonald, Phys. Rev. B **64**, 184423 (2001).
- ³¹ G. Bouzerar and T. P. Pareek, Phys. Rev. B **65**, 153203 (2002).
- ³² M. Berciu and R. N. Bhatt, Phys. Rev. B **66**, 085207 (2002).
- ³³ W. Nolting, T. Hickel, A. Ramakanth, G. G. Reddy, and

- M. Lipowczam, Phys. Rev. B **70**, 075207 (2004).
- ³⁴ A. Singh and P. Sen, Phys. Rev. B **57**, 10598 (1998).
- ³⁵ K. Sato, P. H. Dederichs, H. Katayama-Yoshida, and J. Kudrnovsky, Physica B **340-342**, 863 (2003).
- ³⁶ B. Sanyal, O. Bengone, and S. Mirbt, Phys. Rev. B **68**, 205210 (2003).